IV Simpósio Paranaense de Modelagem, Simulação e Controle de Processos
ISSN : 1984-7521
Artigo: 23
Páginas: 165 - 172

INFLUENCE OF RHEOLOGICAL MODELS IN A GENERIC CAROTID ARTERY ANEURYSM WITH THE USE OF COMPUTATIONAL HEMODYNAMICS

Cristian Ricardo Schwatz[1*], Igor Augusto Depiné Fiamoncini[1], Carolina Aparecida Sens[1], Ricardo Nava de Sousa[1], Marcela Kotsuka da Silva Câmara Bastos[1], Henry França Meier[1], Jaci Carlo Schramm Câmara Bastos[1]

1 – University of Blumenau – FURB, Blumenau – SC, criistianrs@hotmail.com

Abstract
Aneurysms are deformations that occur in artery walls, due to excessive blood pressure or a decrease in the blood vessel wall resistance. This type of pathology is often seen in intracranial arteries. Thus, once this aneurysm ruptures, it results in an internal haemorrhage, which can consequently lead to death or morbidity of the patient. In order to aid physicians, CFD-based tools can be used to obtain key parameters, such as WSS[1]. Due to the nature of the blood, this fluid behaves as a non-Newtonian fluid. Therefore, this study aimed to compare and analyze the influence of rheological models on the blood flow in an idealized aneurysm in the carotid artery. Results showed that non-Newtonian models have a direct impact on the WSS and that a Newtonian model might underestimate WSS.
Keywords: Hemodynamics; Carotid artery; Aneurysm; Rheological models.

Introduction

Cerebral aneurysms are pathologies in which the artery wall presents an abnormal dilatation. This pathology, which occurs frequently at the circle of Willis, is estimated to affect 2% to 5% of the entire population [1-4]. In cases of non-treatment, aneurysms can rupture, leading to sub-arachnoid hemorrhage [2-4]. Moreover, it is predicted that 2% of all aneurysms will rupture at one point, resulting in a death rate as high as 50% [2]. When its rupture does not lead to death, aneurysms are one of the main causes of strokes, which results in a possible morbidity of the patient [1,6]. Additionally, aneurysms are often asymptomatic, hindering its diagnosis. The causes behind the occurrence, development and even rupture of aneurysms are associated with hemodynamic forces that act on the arterial wall surface [1,5,7]. In order to treat aneurysms, both invasive and non-invasive methods can be applied, depending on the size and location of the dilatation. These treatments are applied with the objective of eliminating the aneurysm from the blood circulation [2,9]. Given that hemodynamic forces have a decisive role in the development of aneurysms, CFD[2] tools have been used along with medical imaging techniques, such as MRI[3] or CT-scans, in order to further analyze the hemodynamics [7-9].

When conducting CFD-based analysis, blood rheology is an important factor to take into consideration, since blood is a suspension-type fluid. This kind of rheology is explained by the fact that blood is composed of solid particles, the blood cells, suspended in the plasma. Due to this nature, the blood presents a shear-thinning behavior [10-12]. Although studies tend to simulate blood as being a Newtonian fluid, since this consideration provides reasonable results [12], it does not follow the real rheological behavior. Thus, this study aims to simulate blood flow in a generic artery with an aneurysm via CFD tools, whilst comparing non-Newtonian rheological models and their impact in hemodynamic factors, such as velocity and wall shear-stress.

[1] WSS – Wall Shear Stress
[2] CFD – Computational Fluid Dynamics
[3] MRI – Magnetic Resonance Imaging

Experimental

In order to make the simulations possible, a generic 3D geometry was built based on geometric data from a common carotid artery and a generic aneurysm [13,14]. Therefore, both the artery and the aneurysm had idealized geometries, as seen in Fig. 1. Using the geometry developed, a numerical mesh with 665 thousand elements was created to discretize the space and solve the conservation equations. To facilitate the evaluation of the results, cross sectional planes were drawn in this geometry, which can also be seen in Fig 1. From Fig. 1, it is also possible to observe that the aneurysm drawn is located in the CCA[4], which classifies it as being an extracranial aneurysm. Although extracranial aneurysms have rare occurrence rates of 0.4%-4% [16,17], this position was chosen as being a primary study, given that the bifurcation will not interfere in the flow entering the aneurysm.

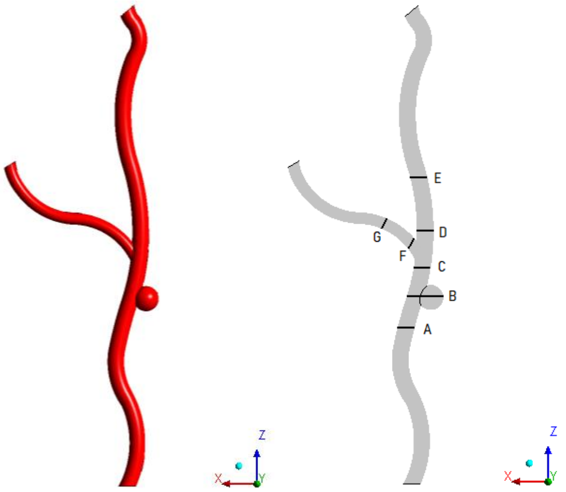

Figure 1 – Generic geometry and cross sectional planes of analysis in relation to the bifurcation: A - 20mm below; B – 11 mm below; C – 2 mm below; D – 2 mm above ; E – 11 mm above; F – 2 mm above; G – 10 mm above.

After the pre-processing, the simulations were computed in a computer with the following specifications: Intel Core i7-4700HQ 2.40GHz. All stages of the simulation were carried in a commercial software provided by ANSYS®.

During the processing stage, rheological model equations were fed to the software via the use of UDFs[5] so the comparison among models could be possible. As an inlet boundary condition, constant velocity was adopted at the entrance of the CCA. For the other boundary conditions, no-slip was adopted on the walls and arterial pressure was adopted as outlet conditions for the ICA[6] and ECA[7]. The parameters used in the simulations are presented in Table 1. Additionally, all simulations were done for a total time of 4 s, with a time step of 10^{-3} s.

Table 1 – Simulation parameters fed to the software.

Parameter	Symbol	Value
Density	ρ	1050 kg/m^3
Viscosity	μ	0.004 Pa.s
Velocity	u	0.5 m/s
Arterial Pressure	P_a	13332.24 Pa

[4] CCA – Common Carotid Artery
[5] UDFs – User Defined Functions
[6] ICA – Internal Carotid Artery
[7] ECA – External Carotid Artery

The conservation equations (Eq. 1,2), as well as the rheological models (Eq. 3-8) analyzed are displayed in Table 2. All the models constants and parameters required to use the equations in Table 2 were taken from a previous study [12].

Table 2 – Equations used in the simulations.

Equation	Expression	
Conservation of Mass	$(\boldsymbol{\nabla}\cdot\mathbf{u}) = 0$	(1)
Conservation of Momentum	$\frac{\partial}{\partial t}\rho\mathbf{u} = -[\boldsymbol{\nabla}\cdot\rho\mathbf{uu}] - \boldsymbol{\nabla}p - [\boldsymbol{\nabla}\cdot\boldsymbol{\tau}] + \rho\mathbf{g} + \mathbf{F}$	(2)
Power-Law	$\eta(\dot{\gamma}) = k\dot{\boldsymbol{\gamma}}^{(\mathbf{n-1})}$	(3)
Generalized Power-Law	$\eta(\dot{\gamma}) = k(\dot{\gamma})\dot{\gamma}^{(\mathbf{n}(\dot{\gamma})-\mathbf{1})} \begin{cases} k(\dot{\gamma}) = \eta_\infty + \Delta\eta \exp\left[-\left(1+\frac{\dot{\gamma}}{a}\right)\exp\left(-\frac{b}{\dot{\gamma}}\right)\right] \\ n(\dot{\gamma}) = n_\infty + \Delta n \exp\left[-\left(1+\frac{\dot{\gamma}}{c}\right)\exp\left(-\frac{d}{\dot{\gamma}}\right)\right] \end{cases}$	(4)
Modified Casson	$\eta(\dot{\gamma}) = \left(\sqrt{\eta_C} + \frac{\sqrt{\boldsymbol{\tau}_C}}{\sqrt{\lambda} + \sqrt{\dot{\gamma}}}\right)$	(5)
Carreau-Yasuda	$\eta(\dot{\gamma}) = \eta_\infty + (\eta_0 - \eta_\infty)[1 + (\lambda\dot{\gamma})^a]^{(n-1)/a}$	(6)
Carreau	$\eta(\dot{\gamma}) = \eta_\infty + (\eta_0 - \eta_\infty)[1 + (\lambda\dot{\gamma})^2]^{(n-1)/2}$	(7)
Carreau-Cross	$\eta(\dot{\gamma}) = \eta_\infty + \frac{(\eta_0 - \eta_\infty)}{1 + (\lambda\dot{\gamma})^a}$	(8)

Results and Discussion

Blood flow was simulated in accordance with the procedure presented in the experimental section and results are shown in Table 3, as well as Fig. 2-5.

From Fig. 2 and 3, it can be seen that different rheological models presented barely distinguishable differences for both the axial and cross-sectional velocity profiles. This similarity pattern was noticed in every rheological model, except the Carreau-Cross model, which presented higher values in all the analyzed parameters. This pronounced difference arises from the fact that this model presents a few discrepancies in shear rate ranges below 1 s^{-1} [12]. The same pattern of discrepancies with the Carreau-cross model can be observed when analyzing the WSS.

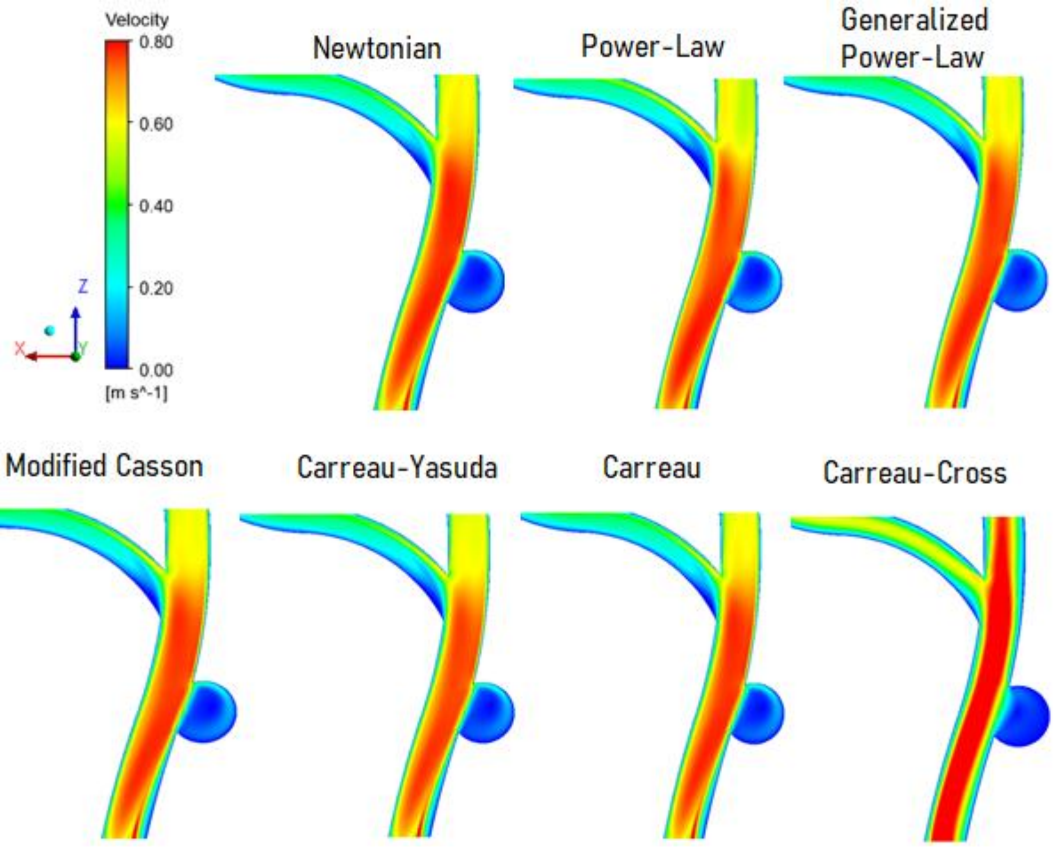

Figure 2 – Axial velocity profiles for all rheological models.

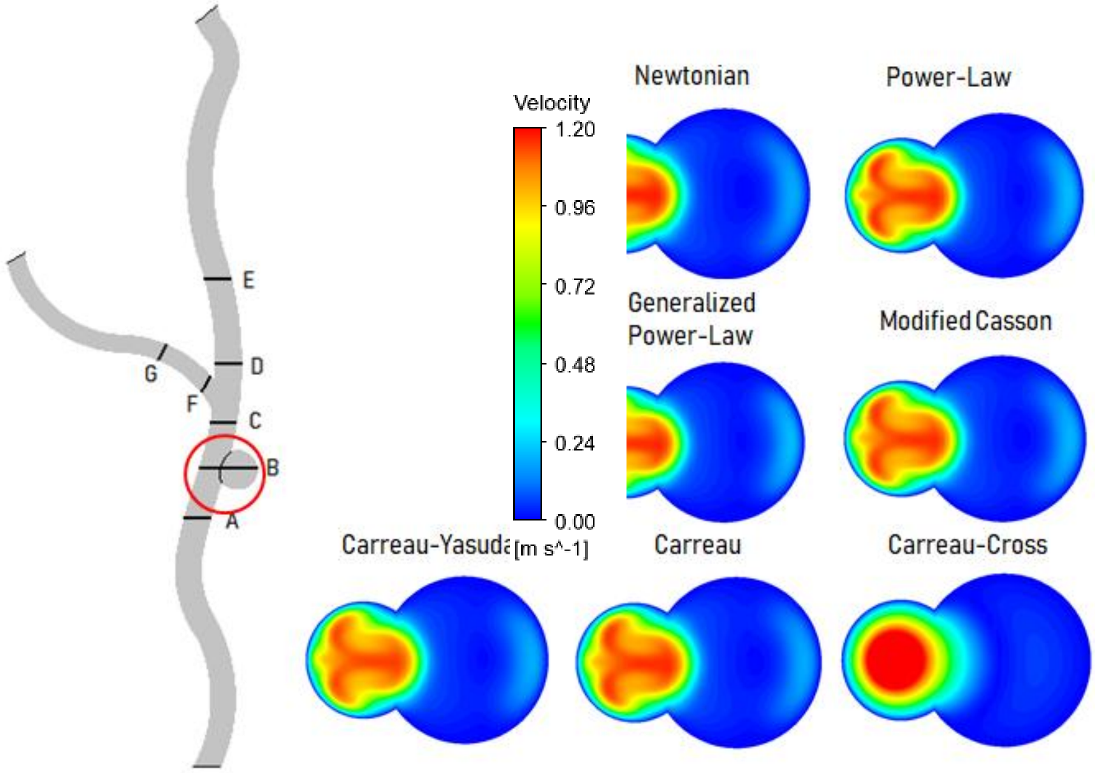

Figure 3 – Radial velocity profiles for all rheological models.

In order to analyze the WSS, a frontal and upper view of the aneurysm are presented in Fig. 4 and 5, given the relevance of identifying low WSS zones to this study. This importance is due to the fact that low WSS zones tend to increase cellular permeability, which results in a higher vulnerability of the arterial wall to atherosclerosis[8] [12].

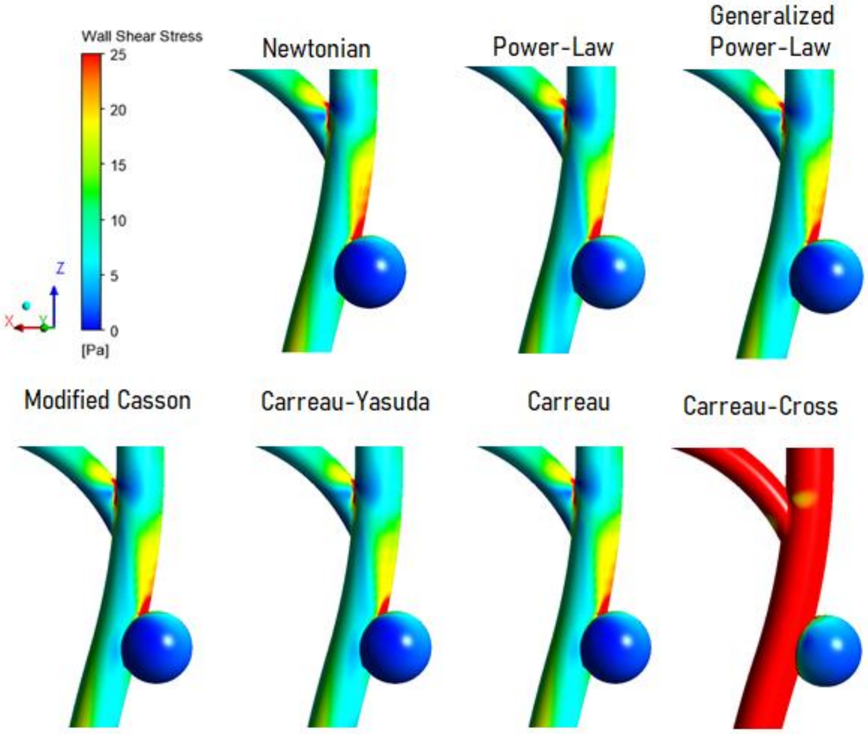

Figure 4 – Frontal view of the WSS in the aneurysm region.

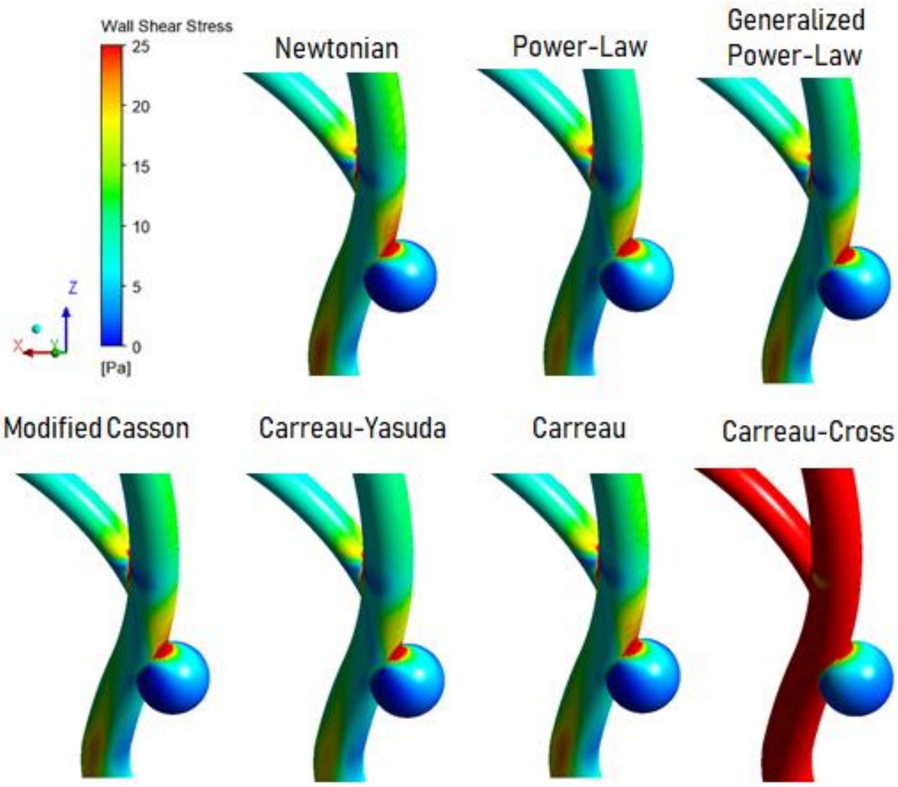

Figure 5 – Upper view of the WSS at the aneurysm region.

[8] Atherosclerosis – A pathology in which an atherosclerotic plaque develops on the artery wall, hindering the blood flow.

Due to the low distinguishability of the Figures presented, Table 3 was made to facilitate the visualization of the differences among the models. As expected, viscosity values showed variations, since viscosity is a function of shear rate. As for the WSS, only the values at the aneurysm were taken into consideration, given that it is the region of interest. Even though WSS values obtained are in an acceptable range, it is important to notice that WSS is highly influenced by the inflow conditions [11,12]. Moreover, WSS values for the Newtonian model are slightly lower than the non-Newtonian models. Hence, the Newtonian model might underestimate WSS in lower ranges, which is in accordance with the literature [12,18].

Table 3 – Results obtained from the simulations.

Rheological Model	**Viscosity (Pa.s)**		**WSS at the Aneurysm (Pa)**
	Minimum	**Maximum**	
Newtonian	0.0040	0.0040	0.627
Power-Law	0.0030	0.0040	1.354
Generalized Power-Law	0.0035	0.0304	0.846
Modified Casson	0.0032	0.0090	0.863
Carreau-Yasuda	0.0025	0.0161	0.930
Carreau	0.0036	0.0158	0.703
Carreau-Cross	0.0364	0.0364	2.117

In Table 4 the non-Newtonian importance factors are presented for each rheological model. This factor indicates quantitatively the divergence of the non-Newtonian model in comparison to the Newtonian, by averaging the local dynamic viscosity and comparing it to the constant Newtonian viscosity [18,19]. Using the cut-off value of 0.25 from the literature [19], it can be seen that the Generalized Power-Law, Carreau-Yasuda and Carreau-Cross are the models that predict the higher viscosities among all the models tested.

Table 4 – non-Newtonian importance factors.

Rheological Model	$\bar{\mathbf{I}}_{\mathbf{G}}$
Power-Law	0.11367
Generalized Power-Law	0.25397
Modified Casson	0.18368
Carreau-Yasuda	0.35592
Carreau	0.21964
Carreau-Cross	9.55073

Conclusion

With the aid of CFD simulations, the impact of rheological models on the blood flow in an idealized carotid artery with an aneurysm was analysed. The simulations showed that using a Newtonian approach might underestimate WSS values in the aneurysm. Furthermore, the Carreau-Cross model presented disparities compared to other non-Newtonian models due to the shear rate range in which the blood is encountered. As for the importance factor, only the Carreau-Yasuda, Generalized

Power-Law and Carreau-Cross models showed results above the cut-off factor, meaning that these models are closer to a non-Newtonian behaviour.

Moreover, WSS values obtained might not represent realistic results, since a pulsatile flow was not adopted in these simulations and inflow boundary conditions directly affect the WSS. Additionally, the geometry developed was idealized, which also contributes to deviation from the real values. Nevertheless, this paper served as initial study for future projects, in which these limitations are being overcome.

Acknowledgements

This study was financed in part by the Coordenação de Aperfeiçoamento de Pessoal de Nível Superior – Brasil (CAPES) – Finance Code 001.

References

[1] L. Xu; F. Liang; L. Gu; H. Liu. Flow instability detected in ruptured versus unruptured cerebral aneurysms at the internal carotid artery. Journal of Biomechanics. 2018, 72, 187-199.

[2] Bernardini; I. Larrabide; H. G. Morales; G. Pennati; L. Petrini; S. Cito; A. F. Frangi. Influence of different computational approaches for stent deployment on cerebral aneurysm haemodynamics. Interface Focus. 2011, 1, 338-348.

[3] P. M. Munarriz; P. A. Gómez; I. Paredes; A. M. Castaño-Leon; S. Cepeda; A. Lagares. Basic Principles of Hemodynamics and Cerebral Aneurysms. World Neurosurgery. 2016, 88, 311-319.

[4] M. Longo; F. Granata; S. Racchiusa; E. Mormina; G. Grasso; G. M. Longo; G. Garufi; F. M. Salpietro; C. Alafaci. Role of Hemodynamics Forces in Unruptured Intraceranial Aneurysms: Na Overview of a Complex Scenario. 2017, 105, 632-642.

[5] M. Castro; C. Putman; A. Radaelli; A. Frangi; J. Cebral. Hemodynamics and Rupture of Terminal Cerebral Aneurysms. Academic Radiology. 2009, 16, 1201-1207.

[6] Shamloo; M. A. Nejad; M. Saeedi. Fluid-structure interaction simulation of a cerebral aneurysm: Effects of endovascular coiling treatment and aneurysm wall thickening. Journal of the Mechanical Behavior and Biomedical Materials. 2017, 74, 72-83.

[7] M. Shojima; M. Oshima; K. Takagi; R. Torii; M. Hayakawa; K. Katada; A. Morita; T. Kirino. Magnitude and Role of Wall Shear Stress on Cerebral Aneurysm. Stroke. 2004, 35, 2500-2505.

[8] M. Li; J. Wang; J. Liu; C. Zhao; X. Yang. Hemodynamics in Ruptured Intracranial Aneurysms with Known Rupture Points. World Neurosurgery. 2018, 118, 721-726.

[9] S. Wang; J. Chen; G. Ding. Non-Newtonian Computational Hemodynamics in Two Patient-Specific Cerebral Aneurysms with Daughter Saccules. Journal of Hydrodynamics. 2010, 22, 639-646.

[10] J. Jung; A. Hassanein. Three-phase CFD analytical modelling of blood flow. 2008, 30, 91-103.

[11] Razavi; E. Shirani; M. R. Sadeghi. Numerical simulation of blood pulsatile flow in a stenosed carotid artery using different rheological models. Journal of Biomechanics. 2011, 44, 2021-2030.

[12] S. Karimi; M. Dabagh; P. Vasava; M. Dadvar; B. Dabir; P. Jalali. Effect of rheological models on the hemodynamics within human aorta: CFD study on CT image-based geometry. Journal of Non-Newtonian Fluid Mechanics. 2014, 207, 42-52.

[13] C. A. Sens. Análise por simulação numérica da hemodinâmica na artéria carótida extracraniana pré e pós angioplastia com *stent.* Masters Thesis, University of Blumenau, 2018.
[14] Hoi, Heng, Woodward, Bendok, Hanel, Guterman, Hopkins (2004).
[15] Holbek, Hansen, Bouzari, Ewertsen, Stuart, Thomsen, Nielsen, Jensen (2017).
[16] G. Song; L. Jiao; Y. Chen; Y. Wang; Y. Ma; F. Ling. Management of extracanial carotid artery aneurysm: A report of four cases. Eperimental and Therapeutic Medicine. 2015, 10, 1029-1032.
[17] G. Altun; Z. Pulathan; D. Hemsinli. True Aneurysms of the Extracranial Carotid Artery: An Evaluation of Two "Giant Aneurysms" and the Current Literature. Journal of Korean Neurosurgery Society. 2018, 61, 282-286.
[18] Skiadopoulus; P. Neofytou; H. Housiadas. Comparison of blood rheological models in patient specific cardiovascular system simulations. Journal of Hydrodynamics. 2017, 29, 293-304.
[19] B. M. Johnston; P. R. Johnston; S. Corney; D. Kilpatrick. Non-Newtonian blood flow in human right coronary arteries: steady state simulations. Journal of Biomechanics. 2004, 37, 709-720.